Robustness of topological order and formation of quantum well states in topological insulators exposed to ambient environment

Chaoyu Chen[a], Shaolong He[a], Hongming Weng[a], Wentao Zhang[a], Lin Zhao[a], Haiyun Liu[a], Xiaowen Jia[a], Daixiang Mou[a], Shanyu Liu[a], Junfeng He[a], Yingying Peng[a], Ya Feng[a], Zhuojin Xie[a], Guodong Liu[a], Xiaoli Dong[a], Jun Zhang[a], Xiaoyang Wang[b], Qinjun Peng[b], Zhimin Wang[b], Shenjin Zhang[b], Feng Yang[b], Chuangtian Chen[b], Zuyan Xu[b], Xi Dai[a], Zhong Fang[a], and X. J. Zhou[a,1]

[a]Beijing National Laboratory for Condensed Matter Physics, Institute of Physics, Chinese Academy of Sciences, Beijing 100190, China; and [b]Technical Institute of Physics and Chemistry, Chinese Academy of Sciences, Beijing 100190, China

Edited by* E. Ward Plummer, Louisiana State University, Baton Rouge, LA, and approved January 18, 2012 (received for review September 24, 2011)

The physical property investigation (like transport measurements) and ultimate application of the topological insulators usually involve surfaces that are exposed to ambient environment (1 atm and room temperature). One critical issue is how the topological surface state will behave under such ambient conditions. We report high resolution angle-resolved photoemission measurements to directly probe the surface state of the prototypical topological insulators, Bi_2Se_3 and Bi_2Te_3, upon exposing to various environments. We find that the topological order is robust even when the surface is exposed to air at room temperature. However, the surface state is strongly modified after such an exposure. Particularly, we have observed the formation of two-dimensional quantum well states near the exposed surface of the topological insulators. These findings provide key information in understanding the surface properties of the topological insulators under ambient environment and in engineering the topological surface state for applications.

The topological insulators represent a novel state of matter where the bulk is insulating but the surface is metallic, which is expected to be robust due to topological protection (1–5). The topological surface state exhibits unique electronic structure and spin texture that provide a venue not only to explore novel quantum phenomena in fundamental physics (6–10) but also to show potential applications in spintronics and quantum computing (2,5,11). The angle-resolved photoemission spectroscopy (ARPES) is a powerful experimental tool to directly identify and characterize topological insulators (12). A number of three-dimensional topological insulators have been theoretically predicted and experimentally identified by ARPES (13–21); some of their peculiar properties have been revealed by scanning tunneling microscopy (STM) (22–26). The application of the topological surface states depends on the surface engineering that can be manipulated by incorporation of nonmagnetic (27–31) or magnetic (27, 28, 31–33) impurities or gas adsorptions (27, 33–35). While the ARPES and STM measurements usually involve the fresh surface obtained by cleaving samples in situ under ultrahigh vacuum, for the transport and optical techniques, which are widely used to investigate the intrinsic quantum behaviors of the topological surface state (36–40), and particularly the ultimate applications of the topological insulators, the surface is usually exposed to ambient conditions (1 atm air and room temperature) or some gas protection environment. It is therefore crucial to investigate whether the topological order can survive under the ambient conditions and, furthermore, whether and how the surface state may be modified after such exposures.

Results and Discussion

We start by first looking at the electronic structure of the prototypical topological insulators $Bi_2(Se,Te)_3$ under ultrahigh vacuum. The Fermi surface and the band structure of the $Bi_2(Se_{3-x}Te_x)$ topological insulators depend sensitively on the composition, x, as shown in Fig. 1. The single crystal samples here were all cleaved in situ and measured at 30 K in an ultrahigh vacuum (UHV) chamber with a base pressure better than 5×10^{-11} torr. For Bi_2Se_3, a clear Dirac cone appears near −0.36 eV (Fig. 1 *D* and *E*); the corresponding Fermi surface (Fig. 1*A*) is nearly circular but with a clear hexagon shape in the measured data (41). It is apparently of n type because the Fermi level intersects with the bulk conduction band. On the other hand, the Dirac cone of the Bi_2Te_3 sample lies near −0.08 eV (Fig. 1 *H* and *I*), much closer to the Fermi level than that reported before (−0.34 eV in ref. 16). The corresponding Fermi surface (Fig. 1*C*) becomes rather small, accompanied by the appearance of six petal-like bulk Fermi surface sheets. These results indicate that our Bi_2Te_3 sample is of p type because the Fermi level intersects the bulk valence band along the $\overline{\Gamma}$-$\overline{M}$ direction. This is also consistent with the positive Hall coefficient measured on the same Bi_2Te_3 sample (42). This difference of the Fermi surface topology and the location of the Dirac cone from others (16) may be attributed to the different carrier concentration in Bi_2Te_3 due to different sample preparation conditions. In our $Bi_2(Se_{3-x}Te_x)$ samples, we have seen a crossover from n-type Bi_2Se_3 to p-type Bi_2Te_3. In order to eliminate the interference of the bulk bands on the surface state near the Fermi level, we fine tuned the composition x in $Bi_2(Se_{3-x}Te_x)$ and found that, for $x = 2.6$, nearly no spectral weight can be discerned from the bulk conduction band, as seen from both the Fermi surface (Fig. 1*B*) and the band structure (Fig. 1 *F* and *G*). A slight substitution of Te by Se in $Bi_2(Se_{0.4}Te_{2.6})$ causes a dramatic drop of the Dirac point to −0.31 eV (Fig. 1 *F* and *G*) and an obvious hexagon-shaped Fermi surface (Fig. 1*B*). It is interesting to note that the hexagon shape of $Bi_2(Se_{0.4}Te_{2.6})$ (Fig. 1*B*) is rather pronounced, although its Fermi surface size is smaller than that of Bi_2Se_3 (Fig. 1*A*). The hexagonally shaped Fermi surface observed in the topological surface states reflects the hybridization of surface electronic states with the bulk states and can be theoretically explained by considering the higher order terms in the $k \cdot p$ Hamiltonian (43).

In order to directly examine how the topological surface state behaves under ambient conditions in the topological insulators,

Author contributions: Chaoyu Chen and X.J.Z. designed research; Chaoyu Chen and H.W. performed research; S.H., W.Z., L.Z., H.L., X.J., D.M., S.L., J.H., Y.P., Y.F., Z. Xie, G.L., X. Dong, J.Z., X.W., Q.P., Z.W., S.Z., F.Y., Chuangtian Chen, and Z. Xu contributed new reagents/analytic tools; Chaoyu Chen, X. Dai, Z.F., and X.J.Z. analyzed data; and Chaoyu Chen and X.J.Z. wrote the paper.

The authors declare no conflict of interest.

*This Direct Submission article had a prearranged editor.

Freely available online through the PNAS open access option.

[1]To whom correspondence should be addressed. E-mail: XJZhou@aphy.iphy.ac.cn.

This article contains supporting information online at www.pnas.org/lookup/suppl/doi:10.1073/pnas.1115555109/-/DCSupplemental.

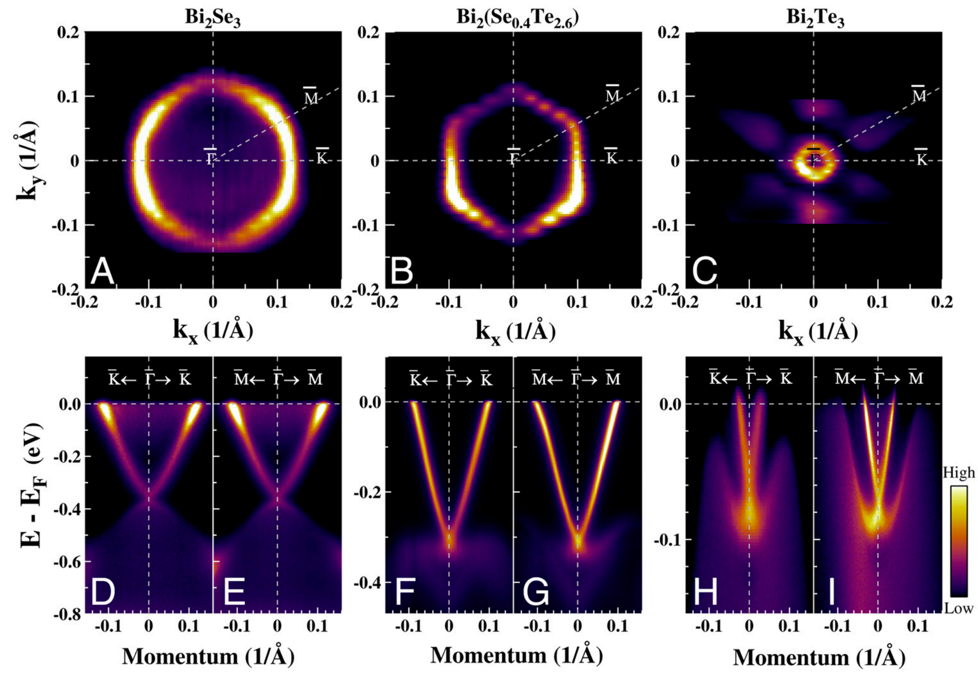

Fig. 1. Fermi surface and band structure of $Bi_2(Se_{3-x}Te_x)$ ($x = 0, 2.6, 3$) topological insulators cleaved in situ and measured at 30 K in ultrahigh vacuum. (*A*–*C*) Fermi surface of Bi_2Se_3, $Bi_2(Se_{0.4}Te_{2.6})$, and Bi_2Te_3, respectively. The Fermi surface here, and in other figures below, are original data without involving artificial symmetrization. The band structures along two high symmetry lines $\bar{\Gamma} - \bar{K}$ and $\bar{\Gamma} - \bar{M}$ are shown in *D* and *E* for Bi_2Se_3, in *F* and *G* for $Bi_2(Se_{0.4}Te_{2.6})$, and *H* and *I* for Bi_2Te_3.

we carried out our ARPES measurements in different ways. (1). We first cleaved the sample in situ and performed ARPES measurement in the ultrahigh vacuum (UHV) chamber. The sample was then pulled out to another chamber filled with 1 atm N_2 gas, exposed for about 5 min, before transferring back to the UHV chamber to do ARPES measurements (2). We cleaved and measured the sample in the UHV chamber and then pulled the sample out to air for 5 min before transferring back to the UHV chamber for the ARPES measurements; (3). We cleaved the sample in air and then transferred it to the UHV chamber to do the ARPES measurement. Our measurements show that the above procedures of exposure to air or N_2 produce similar and reproducible results for a given sample.

The surface exposure of the topological insulators to air or N_2 gives rise to a dramatic alteration of the surface state, as shown in Figs. 2–4, for Bi_2Se_3, $Bi_2(Se_{0.4}Te_{2.6})$, and Bi_2Te_3, respectively, when compared with those for the fresh surface (Fig. 1). The first obvious change is the shifting of the Dirac cone position relative to the Fermi level. For Bi_2Se_3, $Bi_2(Se_{0.4}Te_{2.6})$, and Bi_2Te_3, it shifts from the original −0.36 eV (Fig. 1 *D* and *E*), −0.31 eV (Fig. 1 *F* and *G*), −0.08 eV (Fig. 1 *H* and *I*) for the fresh surface to −0.48 eV (Fig. 2*B*), −0.40 eV (Fig. 3 *A* and *B*), and −0.28 eV (Fig. 4 *C*–*F*) at 30 K for the exposed surface, respectively. In all these cases, the shift of the Dirac cone to a larger binding energy indicates an additional doping of electrons into the surface state. The exposure also gives rise to a dramatic change of the surface-state Fermi surface. For Bi_2Se_3, in addition to a slight Fermi surface size increase, an obvious change occurs in the Fermi surface shape that the hexagon shape becomes much more pronounced in the exposed surface (Fig. 2*D*) than that in the fresh sample (Fig. 1*A*). For $Bi_2(Se_{0.4}Te_{2.6})$, one clearly observes the much-enhanced warping effect in the exposed surface (Fig. 3*C*) when compared with the nearly standard hexagon in the fresh surface (Fig. 1*B*). The most dramatic change occurs for Bi_2Te_3 where

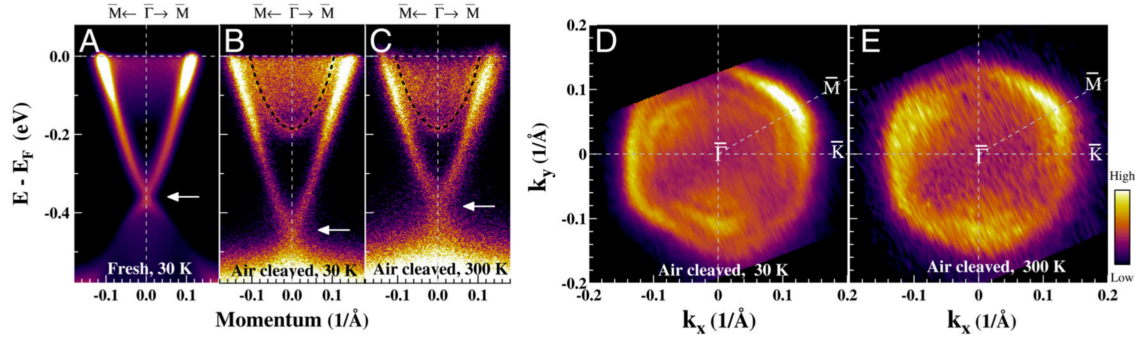

Fig. 2. Fermi surface and band structure of Bi_2Se_3 cleaved in air and measured in the ultrahigh vacuum (UHV) chamber. (*A*) Band structure of the fresh Bi_2Se_3 cleaved and measured in the UHV chamber at 30 K along $\bar{\Gamma} - \bar{M}$ direction. (*B*) Band structure of Bi_2Se_3 cleaved in air and measured in UHV at 30 K along $\bar{\Gamma} - \bar{M}$ direction. (*C*) Band structure of Bi_2Se_3 cleaved in air and measured in UHV at 300 K along $\bar{\Gamma}$-$\bar{M}$ direction. (*D* and *E*) Fermi surface of Bi_2Se_3 cleaved in air and measured in UHV at 30 K and 300 K, respectively. Black dashed lines in *B* and *C* mark the parabolic bands above the Dirac point from the two-dimensional electron gas.

not only the Fermi surface size increases significantly but also the warping effect in the exposed surface (Fig. 4*I*) becomes much stronger. Overall, the exposure causes the lowering of the Dirac cone position, an increase of the surface Fermi surface size, and an obvious enhancement of the Fermi surface warping effect in the $Bi_2(Se_{3-x}Te_x)$ system. A careful comparison of the energy bands and Fermi surface between the fresh and exposed surfaces indicates that, if we take the Dirac cone energy as a common reference energy, the Fermi surface and bands nearly overlap with each other (see Fig. S1). These indicate that the Fermi surface change in the exposed samples is mainly due to chemical potential shift, not from the Fermi surface deformation.

The topological order in the $Bi_2(Se_{3-x}Te_x)$ topological insulators is robust even when the surface is exposed to ambient conditions, in spite of all the alterations mentioned above. One clearly observes the persistence of the Dirac cone in the exposed surface as in Bi_2Se_3 (Fig. 2 *B* and *C*), in $Bi_2(Se_{0.4}Te_{2.6})$ (Fig. 3 *A* and *B*), and Bi_2Te_3 (Fig. 4 *C*–*H*). This is particularly the case for the surface exposed to air and measured at room temperature (Fig. 2*C* for Bi_2Se_3 and Fig. 4 *G* and *H* for Bi_2Te_3). On the other hand, after the exposure, although the signal of the surface state gets weaker for Bi_2Se_3 (Fig. 2), it remains rather strong for $Bi_2(Se_{0.4}Te_{2.6})$ (Fig. 3) and Bi_2Te_3 (Fig. 4). This is in stark contrast to the conventional trivial surface state where minor surface contamination will cause the extinction of the surface state (44). The robustness of the topological order to Coulomb, magnetic, and disorder perturbations has been reported before (33, 34). Our present observations directly demonstrate the robustness of the topological order against absorption and thermal process under ambient conditions, presumably due to the protection of the time-reversal symmetry (3, 4).

The surface exposure to air or N_2 in the $Bi_2(Se_{3-x}Te_x)$ topological insulators produces two-dimensional electronic states near the surface. In Bi_2Se_3, the exposure gives rise to additional parabolic bands, as schematically marked by the dashed line in

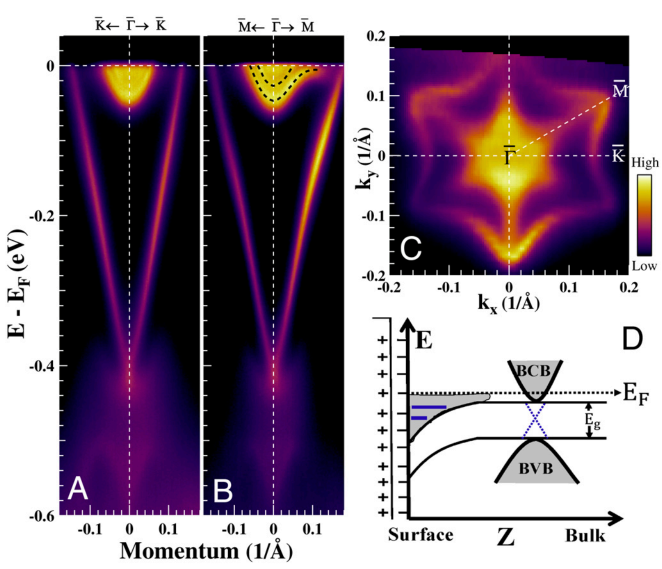

Fig. 3. Emergence of quantum well states in $Bi_2Te_{2.6}Se_{0.4}$ after exposing to N_2. (*A* and *B*) Band structure measured at 30 K along $\bar{\Gamma} - \bar{K}$ and $\bar{\Gamma}$-$\bar{M}$, respectively. Black dashed lines in *B* mark the quantum well states formed in the bulk conduction band (BCB) above the Dirac point. (*C*) The corresponding Fermi surface. It shows threefold symmetry where three corners of M points are strong while the other three are weak. This is also in agreement with the asymmetric band structure in Fig. 3*B*. (*D*) Schematic band structure showing the possible formation of the quantum well states near the sample surface in the bulk conduction band. The blue dotted lines between the bulk valence band (BVB) and bulk conduction band (BCB) represent the topological surface states while the blue solid lines represent quantum well states.

Fig. 2 *B* and *C*. Correspondingly, this leads to additional Fermi surface sheet(s) inside the regular topological surface state (Fig. 2 *D* and *E*). In $Bi_2(Se_{0.4}Te_{2.6})$, this effect gets more pronounced and the newly emerged bulk conduction band splits into several discrete bands, as marked by the dashed lines in Fig. 3*B*. While the band quantization effect occurs in the bulk conduction band in $Bi_2(Se_{0.4}Te_{2.6})$, it shows up in the valence band in the exposed Bi_2Te_3 surface, as shown in Fig. 4 *C*–*H*, where one can see a couple of discrete M-shaped bands. The quantized bands are obvious at low temperature and get slightly smeared out when the temperature rises to room temperature (Fig. 4 *G* and *H*). One may wonder whether these two-dimensional electronic states might come from the formation of a different phase on the surface due to the exposure. We believe this is unlikely because, as shown in Figs. 3 and 4, the two-dimensional electronic states are rather different although the composition of $Bi_2(Se_{0.4}Te_{2.6})$ is only slightly different from Bi_2Te_3.

It is interesting to note that the Dirac structure shows an obvious change with temperature. As shown in Fig. 2 *B* and *C*, as the measurement temperature increases from 30 K to 300 K, the Dirac cone location of Bi_2Se_3 shifts upward from −0.48 eV to −0.38 eV. For Bi_2Te_3, the Dirac cone also shifts to lower binding energy upon increasing temperature from −0.28 eV at 30 K (Fig. 4*E*) to −0.25 eV at 300 K (Fig. 4*G*). On the other hand, the two-dimensional quantum well states show little change with temperature, as shown in Fig. 2 *B* and *C* for Bi_2Se_3. The upward energy shift of the Dirac cone with increasing temperature is possibly due to desorption process on the sample surface which results in electron removal from the surface.

The formation of the split bands in the exposed surface of the topological insulators is reminiscent of the quantum well states observed in the quantum confined systems (45) and in some topological insulators (29–31, 35, 46, 47). There are a couple of possibilities that the quantum well states may be formed. One usual way is due to the band-bending effect. The surface exposure to air or N_2 causes an electron transfer to the surface of the topological insulators. The accumulation of these additional electrons near the surface would lead to a downward bending of the bulk bands near the surface region, as schematically shown in Fig. 3*D*, resulting in a V-shaped potential well where the bulk conduction band of electrons can be confined. This picture, as proposed before (29, 46), becomes questionable to explain the present observation.

Generally speaking, this is because the valence band top has a hole-like component, so the downward band-bending that acts as a quantum well potential for electrons will no longer be a potential for holes. Specifically, Bianchi et al. (29) argued that, when the total bandwidth of the valence band is narrower than the band-bending depth, it is possible to form quantum well states for the valence bands. This scenario does not work for our Bi_2Te_3 case for a couple of reasons. First, although the M-shaped valence band has a V-shape in the middle that acts like electrons and could get quantum well states, the two wings of the bands remain hole-like and they should not generate quantum well states. This is not consistent with the experimental observations that the entire M-shaped band exhibits quantum well states. Second, as pointed out in ref. 29, in order for the band-bending picture to work for the valence band, a necessary condition is that the total bandwidth of the valence band must be smaller than the band-bending depth. This condition is not satisfied in Bi_2Te_3. As seen in Fig. S2, our measured band width of Bi_2Te_3 along the Γ-K direction is 300 meV (Fig. S2*A*). The band structure calculations give a band width along the Γ-K direction of 350 meV (Fig. S2*B*) (16). Using a similar procedure as in ref. 29, the band-bending depth is 227 meV as determined from the position difference of the Dirac point between the freshly cleaved sample (Fig. 4*A*) and the exposed sample (Fig. 4*B*). Therefore, the total bandwidth of Bi_2Te_3 valence band is obviously larger than that of the band-

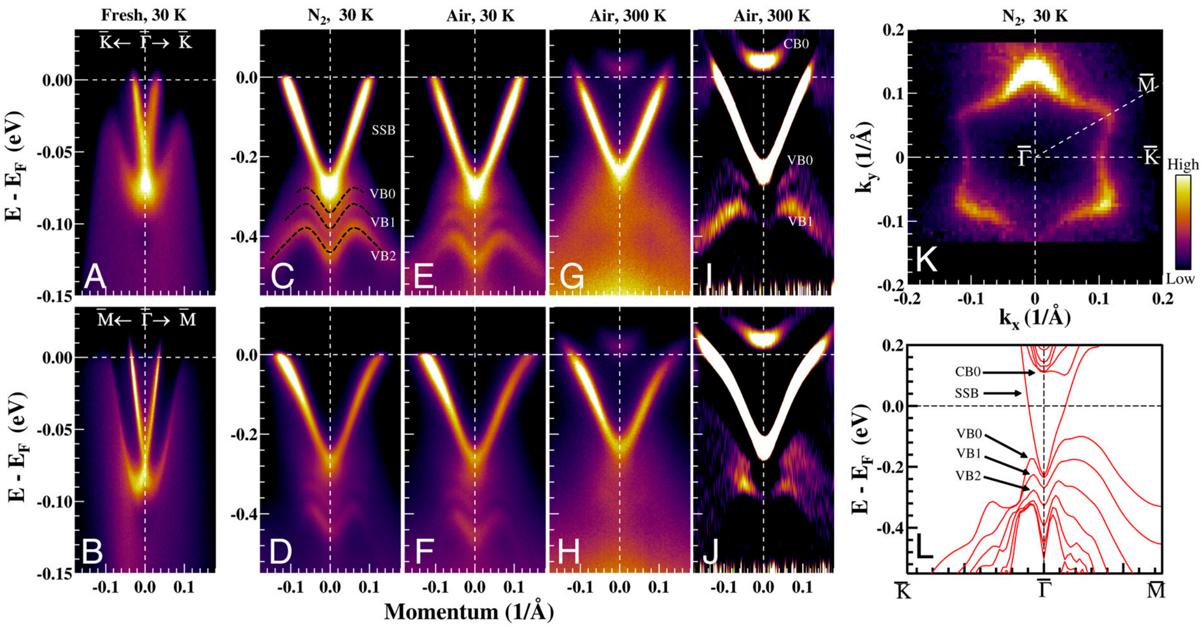

Fig. 4. Persistence of topological surface state and formation of quantum well states in Bi_2Te_3 after exposure to N_2 or air. The sample was first cleaved and measured in UHV at 30 K. (*A* and *B*) The corresponding band structure along the $\bar{\Gamma}$-$\bar{K}$ and $\bar{\Gamma}$-$\bar{M}$ directions. The sample was then pulled out from the UHV chamber and exposed to N_2 at 1 atm for 5 min before transferring back into UHV chamber for the ARPES measurement. (*C* and *D*) The band structure of the N_2-exposed sample along the $\bar{\Gamma}$-$\bar{K}$ and $\bar{\Gamma}$-$\bar{M}$ directions. The black dashed lines in *C* illustrate the quantum well states formed in the bulk valence band below the Dirac point. The sample was then pulled out again and exposed to air for 5 min before putting back in vacuum for ARPES measurement. (*E* and *F*) The band structure of the air-exposed sample at 30 K along the $\bar{\Gamma}$-$\bar{K}$ and $\bar{\Gamma}$-$\bar{M}$ directions. (*G* and *H*) The measurements at 300 K, and *I* and *J* show their corresponding second-derivative images in order to highlight the bands. (*K*) Fermi surface of N_2-exposed sample. (*L*) First principle calculation of the band structure of Bi_2Te_3 slab with seven quintuple layers.

bending depth, which does not satisfy the necessary requirement proposed in ref. 29. The observation of quantum well states in the valence band of Bi_2Te_3 cannot be explained by the picture proposed in ref. 29. Therefore, the band-bending is not a general picture to explain the formation of the quantum well states in all the samples on the same footing.

An alternative scenario is the expansion of van der Waals spacings in between the quintuple layers (QLs) caused by the intercalation of gases (48). The observation of multiple split bands with different spacings would ask for multiple van der Waals gaps with different expansions. Whether and how these can be realized in the exposed surface remains to be investigated. We note that our observations of multiple split bands are similar to those seen in the ultrathin films of Bi_2Se_3 (49) and Bi_2Te_3 (50). From our first principle band structure calculations on Bi_2Te_3 with different number of quintuple layers, we also find that a detached slab with a thickness of seven quintuple layers can give a rather consistent description (Fig. 4*L*) of our observed results in terms of the quantitative spacings between the three resolved bands (VB0, VB1, and VB2 bands as marked in Fig. 4 *C* and *L*). In addition, the distance between the conduction band bottom (CB0 band in Fig. 4 *I* and *L*) and the first valence subband bottom (VB0 band in Fig. 4 *I* and *L*) is rather consistent between the measured and calculated results. These seem to suggest that a “confined surface slab” with nearly seven quintuple layers may be formed after the exposure that acts more or less independently from the bulk. More work needs to be done to further investigate whether such a confined surface slab can be thermodynamically stable. Overall, the formation of the two-dimensional quantum well states is a general phenomenon for the exposed surface of the $Bi_2(Se_{3-x}Te_x)$ topological insulators; the effect depends sensitively on the composition x of the samples, which may facilitate manipulation of these quantum well states.

The present work has significant implications on the fundamental study and ultimate applications of the topological insulators. Many experimental measurements, such as some transport measurements, involve samples exposed to ambient conditions. The practical applications may involve sample surface either exposed to ambient condition or in contact with other magnetic or superconducting materials. On the one hand, the robustness of the topological order under ambient conditions sends a good signal for these experimental characterization and practical utilizations. The formation of the quantum well states may give rise to new phenomena to be studied and utilized. The sensitivity of the surface state to the $Bi_2(Se_{3-x}Te_x)$ composition provides a handle to manipulate these quantum states. On the other hand, the strong modification of the electronic structure and the formation of additional quantum well states in the exposed surface have to be considered seriously in interpreting experimental data and in surface engineering. The observed change of resistivity and Hall coefficient with time can be understood as a result of electron doping on the air-exposed surface (51). It is critical to realize beforehand that the surface under study or to be utilized may exhibit totally different behaviors as those from the fresh surface cleaved in ultrahigh vacuum. In addition to the alteration of electronic states upon exposure, the transport properties of the topological surface state may be further complicated by the formation of quantum well states. In this sense, the transport measurements need to be checked because no considerations were made before on the formation of quantum well states that may affect transport analysis (36–39).

Methods

Crystal Growth Methods. Single crystals of $Bi_2(Se_{3-x}Te_x)$ ($x = 0$, 2.6, and 3) were grown by the self-flux method. Bismuth, selenium, and tellurium powders were weighed according to the stoichiometric $Bi_2(Se_{3-x}Te_x)$ ($x = 0$, 2.6, and 3) composition. After mixing thoroughly, the powder was placed in alumina crucibles and sealed in a quartz tube under vacuum. The materials were heated to 1,000 °C, held for 12 h to obtain a high degree of mixing, and then slowly cooled down to 500 °C over 100 h before cooling to room temperature. Single crystals of several millimeters in size were obtained. The crystal structure of the resulting crystals was examined by use of a rotating anode X-ray diffractometer with Cu $K\alpha$ radiation ($\lambda = 1.5418$ Å). The chemical composition of the crystals was analyzed by the energy dispersive X-ray spectroscopy (EDAX) and the induction-coupled plasma atomic emission spectroscopy (ICP-AES). The resistivity of the crystals was measured by the standard four-probe method.

Laser-ARPES Methods. The angle-resolved photoemission measurements were carried out on our vacuum ultraviolet (VUV) laser-based angle-resolved photoemission system (52). The photon energy of the laser is 6.994 eV with a bandwidth of 0.26 meV. The energy resolution of the electron energy analyzer (Scienta R4000) is set at 1 meV, giving rise to an overall energy resolution of approximately 1 meV, which is significantly improved from $10\sim15$ meV from regular synchrotron radiation systems (15, 16). The angular resolution is approximately 0.3°, corresponding to a momentum resolution of approximately 0.004 $\mathrm{Å}^{-1}$ at the photon energy of 6.994 eV, more than twice improved from 0.009 $\mathrm{Å}^{-1}$ at a regular photon energy of 21.2 eV for the same angular resolution. Our superior instrumental resolution of laser ARPES has made the measured features of topological insulators in this work much sharper. The Fermi level is referenced by measuring on a clean polycrystalline gold that is electrically connected to the sample. The samples were all measured in vacuum with a base pressure better than 5×10^{-11} torr.

ACKNOWLEDGMENTS. We thank Prof. Xianhui Chen for providing us samples at the initial stage of the project and Prof. Liling Sun and Prof. Zhong-xian Zhao for their help in the characterization of the samples. This work is supported by the National Natural Science Foundation of China (91021006) and the Ministry of Science and Technology of China (973 program 2011CB921703).

1. Fu L, Kane CL, Mele EJ (2007) Topological insulators in three dimensions. *Phys Rev Lett* 98:106803.
2. Qi XL, Zhang SC (2010) The quantum spin Hall effect and topological insulators. *Phys Today* 63:33–38.
3. Hasan MZ, Kane CL (2010) Colloquium: Topological insulators. *Rev Mod Phys* 82:3045–3067.
4. Qi X-L, Zhang S-C (2011) Topological insulators and superconductors. *Rev Mod Phys* 83:1057–1110.
5. Moore JE (2010) The birth of topological insulators. *Nature* 464:194–198.
6. Qi X-L, Hughes TL, Zhang S-C (2008) Fractional charge and quantized current in the quantum spin Hall state. *Nat Phys* 4:273–276.
7. Li R, Wang J, Qi X-L, Zhang S-C (2010) Dynamical axion field in topological magnetic insulators. *Nat Phys* 6:284–288.
8. Qi X-L, Li R, Zang J, Zhang S-C (2009) Inducing a magnetic monopole with topological surface states. *Science* 323:1184–1187.
9. Fu L, Kane CL (2008) Superconducting proximity effect and Majorana fermions at the surface of a topological insulator. *Phys Rev Lett* 100:096407.
10. Yu R, et al. (2010) Quantized anomalous Hall effect in magnetic topological insulators. *Science* 329:61–64.
11. Moore J.E (2009) Topological insulators the next generation. *Nat Phys* 5:378–380.
12. Hasan MZ (2011) A new experimental approach for the exploration of topological quantum phenomena. http://arxiv.org/abs/1105.0396.
13. Hsieh D, et al. (2008) A topological Dirac insulator in a quantum spin Hall phase. *Nature* 452:970–974.
14. Zhang HJ, et al. (2009) Topological insulators in Bi_2Se_3, Bi_2Te_3 and Sb_2Te_3 with a single Dirac cone on the surface. *Nat Phys* 5:438–442.
15. Xia Y, et al. (2009) Observation of a large-gap topological insulator class with a single Dirac cone on the surface. *Nat Phys* 5:398–402.
16. Chen YL, et al. (2009) Experimental realization of a three-dimensional topological insulator, Bi_2Te_3. *Science* 325:178–181.
17. Yan BH, et al. (2010) Theoretical prediction of topological insulators in thallium-based III-V-VI2 ternary chalcogenides. *Europhys Lett* 90:37002.
18. Lin H, et al. (2010) Single-Dirac-cone topological surface states in the $TlBiSe_2$ class of topological semiconductors. *Phys Rev Lett* 105:036404.
19. Kuroda K, et al. (2010) Experimental realization of a three-dimensional topological insulator phase in ternary chalcogenide $TlBiSe_2$. *Phys Rev Lett* 105:146801.
20. Sato T, et al. (2010) Direct evidence for the Dirac-cone topological surface states in the ternary chalcogenide $TlBiSe_2$. *Phys Rev Lett* 105:136802.
21. Chen YL, et al. (2010) Single Dirac cone topological surface state and unusual thermoelectric property of compounds from a new topological insulator family. *Phys Rev Lett* 105:266401.
22. Zhang T, et al. (2009) Experimental demonstration of topological surface states protected by time-reversal symmetry. *Phys Rev Lett* 103:266803.
23. Roushan P, et al. (2009) Topological surface states protected from backscattering by chiral spin texture. *Nature* 460:1106–1109.
24. Alpichshev Z, et al. (2010) STM imaging of electronic waves on the surface of Bi_2Te_3: Topologically protected surface states and hexagonal warping effects. *Phys Rev Lett* 104:016401.
25. Cheng P, et al. (2010) Landau quantization of topological surface states in Bi_3Se_3. *Phys Rev Lett* 105:076801.
26. Hanaguri T, et al. (2010) Momentum-resolved Landau-level spectroscopy of Dirac surface state in Bi_2Se_3. *Phys Rev* 82:081305 (R).
27. Wray LA, et al. (2011) Electron dynamics in topological insulator based semiconductor-metal interfaces (topological p-n interface based on Bi_2Se_3 class). http://arxiv.org/abs/1105.4794.
28. Beidenkopf H, et al. (2011) Spatial fluctuations of helical Dirac fermions on the surface of topological insulators. *Nat Phys* 7:939–943.
29. Bianchi M, et al. (2011) Simultaneous quantization of bulk conduction and valence states through adsorption of nonmagnetic impurities on Bi_2Se_3. *Phys Rev Lett* 107:086802.
30. Zhu ZH, et al. (2011) Rashba spin-splitting control at the surface of the topological insulator Bi_2Se_3. *Phys Rev Lett* 107:186405.
31. Pan Z-H, et al. (2011) Scattering on magnetic and non-magnetic impurities on a surface of a topological insulator. http://arxiv.org/abs/1104.0966.
32. Chen YL, et al. (2010) Massive Dirac Fermion on the surface of a magnetically doped topological insulator. *Science* 329:659–662.
33. Wray LA, et al. (2011) A topologocal i nsulator surface under strong Coulomb, magnetic and disorder perturbations. *Nat Phys* 7:32–37.
34. Plucinski L, et al. (2011) Robust surface electronic properties of topological insulators: Bi_2Te_3 films grown by molecular beam epitaxy. *Appl Phys Lett* 98:222503.
35. Benia HM, Lin C, Kern K, Ast CR (2011) Reactive chemical doping of the Bi_2Se_3 topological insulator. *Phys Rev Lett* 107:177602.
36. Qu D-X, Hor YS, Xiong J, Cava RJ, Ong NP (2010) Quantum oscillations and Hall anomaly of surface states in the topological insulator Bi_2Te_3. *Science* 329:821–824.
37. Analytis JG, et al. (2010) Two-dimensional surface state in the quantum limit of a topological insulator. *Nat Phys* 6:960–964.
38. Ren Z, Taskin AA, Sasaki S, Segawa K, Ando Y (2010) Large bulk resistivity and surface quantum oscillations in the topological insulator Bi_2Te_2Se. *Phys Rev B Condens Matter Mater Phys* 82:241306.
39. Chen J, et al. (2010) Gate-voltage control of chemical potential and weak antilocalization in Bi_2Se_3. *Phys Rev Lett* 105:176602.
40. Hsieh D, et al. (2011) Nonlinear optical probe of tunable surface electrons on a topological insulator. *Phys Rev Lett* 106:057401.
41. Kuroda K, et al. (2010) Hexagonally deformed Fermi surface of the 3D topological insulator Bi_2Se_3. *Phys Rev Lett* 105:076802.
42. Zhang C, et al. (2011) Phase diagram of a pressure-induced superconducting state and its relation to the Hall coefficient of Bi_2Te_3 single crystals. *Phys Rev B Condens Matter Mater Phys* 83:140504.
43. Fu L (2009) Hexagonal warping effects in the surface states of the topological insulator Bi_2Te_3. *Phys Rev Lett* 103:266801.
44. Reinert F, et al. (2001) Direct measurements of the L-gap surface states on the (111) face of noble metals by photoelectron spectroscopy. *Phys Rev B Condens Matter Mater Phys* 63:115415.
45. Speer NJ, Tang S-J, Miller T, Chiang T-C (2006) Coherent electronic fringe structure in incommensurate silver-silicon quantum wells. *Science* 314:804–806.
46. Bianchi M, et al. (2010) Coexistence of the topological state and a two-dimensional electron gas on the surface of Bi_2Se_3. *Nat Commun* 1:128, 10.1038/ncomms1131.
47. King PDC, et al. (2011) Large tunable Rashba spin splitting of a two-dimensional electron gas in Bi_2Se_3. *Phys Rev Lett* 107:096802.
48. Eremeev SV, et al. (2011) New interpretation of the origin of 2DEG states at the surface of layered topological insulators. http://arxiv.org/abs/1107.3208.
49. Zhang Y, et al. (2010) Crossover of the three-dimensional topological insulator Bi_2Se_3 to the two-dimensional limit. *Nat Phys* 6:584–588.
50. Li YY, et al. (2010) Intrinsic topological insulator Bi_2Te_3 thin films on Si and their thickness limit. *Adv Mater* 22:4002–4007.
51. Taskin AA, Ren Z, Sasaki S, Segawa K, Ando Y (2011) Observation of Dirac holes and electrons in a topological insulator. *Phys Rev Lett* 107:016801.
52. Liu GD, et al. (2008) Development of a vacuum ultraviolet laser-based angle-resolved photoemission system with a superhigh energy resolution better than 1 meV. *Rev Sci Instrum* 79:023105.

Supporting Information

Chen et al. 10.1073/pnas.1115555109

SI Text

1. Band Dispersions of Bi_2Se_3 and Bi_2Te_3 Surface State Before and After Exposure. Fig. S1*A* shows dispersions for the fresh and exposed surfaces of Bi_2Se_3 measured at 30 K. The dispersions are obtained by fitting the momentum distribution curves (MDCs). The dispersion of the fresh surface is shifted downward by 130 meV to make its Dirac point match that of the exposed surface. The dispersions for the fresh and exposed surfaces of Bi_2Te_3 measured at 30 K are shown in Fig. S1*B* where the dispersion of the fresh surface is shifted downward by 227 meV. In both cases, it is found that the dispersions for the fresh and exposed surfaces nearly overlap with each other. These indicate that the Fermi surface change in the exposed samples is mainly due to chemical potential shift, not from the Fermi surface deformation.

2. Band Width of the Valence Band of Bi_2Te_3. Fig. S2*A* shows the band structure of fresh Bi_2Te_3 measured by ARPES along the $\bar{\Gamma}$-$\bar{K}$ direction. The band width of the bulk valence band is approximately 300 meV. Fig. S2*B* shows the band structure of Bi_2Te_3 from the first principle calculations. The corresponding band width along the $\bar{\Gamma}$-$\bar{K}$ direction is approximately 350 meV.

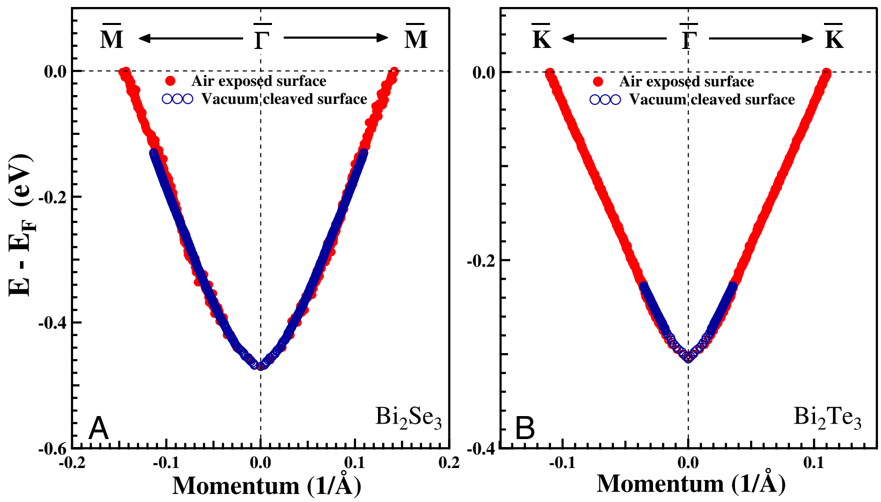

Fig. S1. MDC fitted surface state dispersions of Bi_2Se_3 and Bi_2Te_3. (*A*. MDC fitted dispersions of Bi_2Se_3 along the $\bar{\Gamma}$-$\bar{M}$ direction for the vacuum cleaved surface (blue empty circles) and air-exposed surface (red solid circles). The dispersion of freshly cleaved sample is downward shifted by 130 meV to make its Dirac point match that of the exposed sample. (*B*) MDC fitted dispersions of Bi_2Te_3 along the $\bar{\Gamma}$-$\bar{K}$ direction for the vacuum cleaved surface (blue empty circles) and air-exposed surface (red solid circles). The dispersion of freshly cleaved sample is downward shifted by 227 meV to make the Dirac point coincide with that of the air-exposed surface.

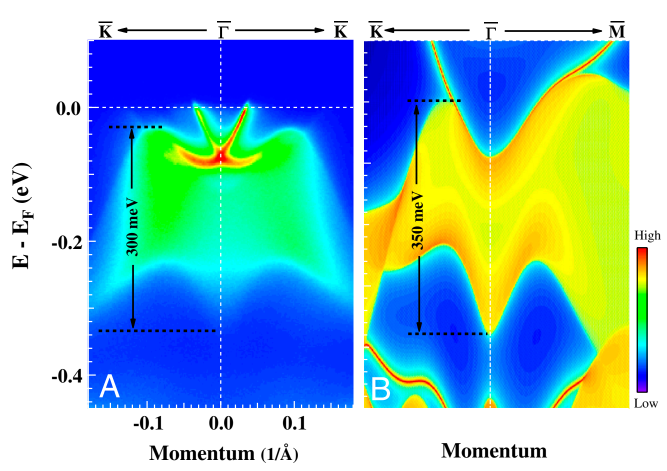

Fig. S2. Band width of bulk valence band in Bi_2Te_3. (*A*) ARPES measured band structure of the vacuum cleaved surface of Bi_2Te_3. The band width of the bulk valence band along the $\bar{\Gamma}$-$\bar{K}$ direction is approximately 300 meV. (*B*) The band structure of Bi_2Te_3 from the first principle calculations. The bandwidth of the bulk valence band is approximately 350 meV.